Thermomechanical Processing Map in Retaining {100}//ND texture *via* Strain-Induced Boundary Migration Recrystallization Mechanism

MO JI, CARL SLATER, and CLAIRE DAVIS

The feasibility of establishing thermomechanical conditions to promote {100}//ND fiber texture *via* strain-induced boundary migration (SIBM) recrystallization mechanism in a non-grain oriented (NGO) electrical steel was investigated. Single-hit uniaxial compression at various temperatures and strains has been applied on Fe-6 wt pct Si to establish the relationship between stored energy and the softening mechanisms. Recovery only and recrystallization by SIBM or by subgrain growth (SGG) have been observed depending on the stored energy level. A strong {100}//ND fiber recrystallization texture, *i.e.*, 45 pct area fraction, was seen in the sample which was deformed to 0.2 strain at 650 °C and then annealed at 1000 °C for 15 minutes, whereas only 13 pct {100}//ND fiber component was observed after 0.4 strain at 500 °C followed by the same annealing treatment. By examining the same microstructural region before and after annealing *via* EBSD, it has been shown that {100}//ND textured recrystallized grains were formed adjacent to the {100}// ND textured deformed matrix. Low stored energy has been shown to favor the formation of {100}//ND texture recrystallized grains *via* SIBM recrystallization mechanism attributed to its slow recrystallization nucleation rate. The results from the deformation studies have been used to suggest a processing window map concept to define the recovery, SIBM, and SGG regions for the starting as-cast columnar microstructure.

https://doi.org/10.1007/s11661-020-06047-x

I. INTRODUCTION

TEXTURE significantly affects the final magnetic properties of electrical steel. {100}//ND texture is desirable for non-grain oriented (NGO) electrical steels. Humphreys and Hatherly summarized that the {100}// ND texture is a minor recrystallization texture attributed to its low nucleation rate and growth rate during recrystallization with subgrain growth (SGG) recrystallization mechanism.[1] Strain-induced boundary recrystallization migration (SIBM) occurs when pre-existing grain boundaries are bulging into a neighboring grain with a higher dislocation density. Dislocations will be swept up during boundary movement. Rosenberg *et al.* reported that {100}//ND fiber texture components have the lowest Taylor factors, whereas grains with {111}// ND texture have relatively high Taylor factors.[2] That is, grains with {100}//ND fiber texture carry less stored energy compared to grains with {111}//ND texture after deformation, for similar grain sizes. As a result, {100}// ND textured grains are expected to be promoted during SIBM recrystallization.

Warm deformation has been studied extensively as a feasible processing route for Fe-6 wt pct Si steel. Mo *et al.* reported that the warm rolling temperature range varies from 400 °C to 700 °C to overcome poor plasticity during cold rolling as well as to minimize oxidation and dimensional distortion during hot deformation.[3] Humphreys *et al.* commented that SIBM is known to occur particularly at low strains and after high-temperature deformation, *i.e.*, low stored energy conditions.[4] Takashima *et al.* reported that {001} ⟨210⟩ textured grains bulged into the adjacent grains *via* SIBM recrystallization after cold rolling (12 pct reduction) in the central region of a partially recrystallized NGO electrical steel sheet.[5] Stojakovic *et al.* also observed that SIBM recrystallization occurred in electrical steels after warm rolling at 350 °C by 12 pct with intermediate annealing at 760 °C, and the {100}//ND textured grains were promoted after recrystallization.[6] Although these studies have been carried out to retain {100}//ND texture *via* SIBM recrystallization in electrical steels, no thermomechanical mapping relating the strain and deformation temperatures to the different softening mechanisms, *i.e.*, recovery, SIBM, and subgrain growth (SGG) mechanism have been established.

MO JI is with the University of Warwick, Coventry CV4 7AL, UK and also with the Brunel University London, Kingston Lane, Uxbridge UB8 3PH, UK. Contact e-mail: Mo.Ji@brunel.ac.uk CARL SLATER and CLAIRE DAVIS are with the University of Warwick.

Manuscript submitted May 26, 2020; accepted September 25, 2020. Article published online October 21, 2020

In this paper, the recovery and recrystallization behavior in Fe-6 wt pct Si steel with a starting columnar {100}//ND texture at various strains and deformation temperatures have been considered, and the concept of a processing map to promote SIBM mechanism has also been established. Other processing parameters, *i.e.*, reheating rate and annealing temperature have also been reported to affect the recrystallization texture. Fang *et al.* and Wang *et al.* observed that both {111}// ND texture fraction and recrystallized grain size decreased with increasing heating rate ranging from 50 °C to 300 °C/s.[7] Jiao *et al.* reported that the {110}//RD texture was strengthened by increasing annealing temperature from 900 °C to 1200 °C.[8] He *et al.* observed that cube texture formed when annealing temperature increased from 600 °C to 750 °C after cross-rolling.[9] These parameters will not be discussed in this paper, with a constant reheating and annealing temperature used, as the main focus in this study is to establish the effect of deformation temperature and strain on the recrystallization texture. The work has initially considered the effect of the strain and temperature on the recrystallization mechanism for columnar-grained samples with one initial grain size, using a single-hit uniaxial compression condition with a strain rate of 1 s^{-1}. The condition chosen is to represent a twin-roll cast strip that could then be processed warm rolling.

II. EXPERIMENT

30-mm-thick slab was cast in a vacuum induction melting furnace. The slab composition is a binary alloy of Fe-6 wt pct Si steel where other elements are below the detectable limits by optical emission spectroscopy. An EBSD map of the as-cast microstructure is shown in Figure 1(a). IPF *Z* coloring used throughout this paper is shown in Figure 1(b). A mixture of columnar (from the mold surface to approximately 9 to 10 mm depth) and equiaxed grains (in the central region of the as-cast slab) microstructure is shown. Columnar grains are 1.2 mm in width with dominant {100}//ND texture. Equiaxed grains vary between 1 and 2 mm in diameter with random texture. The area fraction of the columnar grain region in the compression sample shown is 61 pct. Strain inhomogeneity is expected on compression, as the central region of a uniaxial compression sample known to experience higher strain (depending on the friction conditions at the anvils) and due to the large grain size, grain morphology, and texture. Only the central region of the uniaxial tested samples (which has approximately uniform strain), *i.e.*, approximately 5 × 5 mm, was examined to allow direct comparison between the different conditions.

Cylindrical samples for uniaxial compression tests were machined from the as-cast ingot by electrical discharge machining. The dimension was 10 mm in diameter and 15 mm in height before deformation. The sample compression axis is parallel to ⟨100⟩ direction of the columnar grains. Uniaxial compression samples were then deformed by Gleeble HDS-V40 thermomechanical simulator. The samples were heated to the

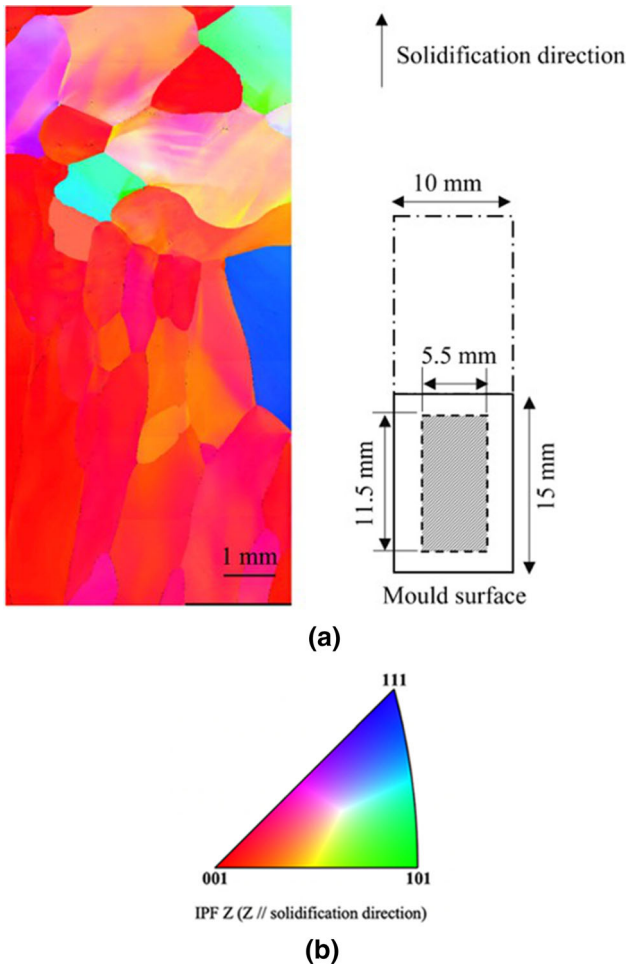

Fig. 1—(*a*) EBSD IPF *Z* mapping and schematic diagram of the examined area (shadow region 11.5 mm × 5.5 mm) of a uniaxial compression sample prior to deformation (half thickness with the mold surface at the bottom of the schematic diagram) showing the initial microstructure consisting of equiaxed and columnar grains. (*b*) IPF *Z* coloring, where *Z* axis is parallel to the solidification direction (Color figure online).

deformation temperature of 500 °C to 700 °C at a heating rate of 20 °C/s, and the deformation strain was between 0.1 and 0.4. The deformation temperatures of the single-hit deformation were selected based on reports that cracking occurs at deformation temperatures less than about 450 °C.[3] These conditions were chosen to demonstrate the effect of different stored energy on the softening mechanisms and annealing texture. The deformed samples were then sectioned along the compression axis for microstructure and texture determination. The deformed samples were polished by the Buehler AutoMet polisher with MasterPrep Alumina suspension. Electron backscattered diffraction (EBSD) analysis was carried out to establish the deformed microstructure. JEOL 7800 FEG-SEM with an OXFORD instrument EBSD system has been applied in this paper. The step size was set to 10 μm, and tolerance was set to 15 deg for orientation indexing. Final annealing was then carried out at 1000 °C for 15 minutes in an argon atmosphere, and the heating rate

was 20 °C/s. The annealed samples were then repolished by using Buehler Microcloth with MasterPrep Alumina suspension for 5 minutes. ESBD mapping was then applied to the annealed samples at the same previous examined region to reveal the texture evolution before and after annealing. One uniaxial compression sample for each condition was assessed, with an area of 25 mm^2 being characterized by EBSD. For each sample, the area fraction of columnar grains (and hence with {100} texture) was between 52 and 64 pct. Due to the large columnar grain size, approximately 15 as-cast columnar grains for each sample were mapped to monitor the texture evolution, with exactly the same area being characterized after deformation and after annealing. Therefore, the starting condition (grain size and texture) microstructure for all tests is the same, meaning that the differences in texture for the recrystallized grains are due to the deformation/annealing conditions. Due to the typically small size of the recrystallized grains (100 to 500 μm), a larger number of recrystallized grains are assessed for most conditions (recrystallized fractions are typically $>$ 65 pct and number of recrystallized grains assessed $>$ 150).

III. RESULTS

Figure 2 summarizes the flow stress curves of Fe-6 wt pct Si steel from 500 °C to 700 °C at a strain rate of 1 s^{-1}. It can be seen that generally the flow stress decreases with increasing temperature and different behaviors are observed for the different test temperatures: the flow stress curve at 500 °C shows an increasing stress characteristic of work hardening; the flow stress curve at 550 °C shows softening after the peak stress, characteristic of dynamic recrystallization, while the flow stress curve at 600 °C to 700 °C shows a relatively flat response after yielding characteristic of dynamic recovery. Dynamic recovery and recrystallization are expected at higher temperatures (typically above half the melting temperature, which is 583 °C for Fe-6 wt pct Si steel).[1] It appears from Figure 2 that dynamic recovery readily occurs at 600 °C to 700 °C attributed to the high stacking fault energy of bcc ferrite.[10] However, at 550 °C it appears that the critical strain for dynamic recrystallization is reached, which may be due a lower extent of dynamic recovery at the lower temperature. At 500 °C, dynamic recovery and/or recrystallization does not occur and only work hardening is seen. Mo *et al.* summarized that Fe-6 wt pct Si steel typically contains ordered B_2 or D_{03} phases, which makes the material brittle at low temperatures.[3] Liu *et al.* and Wen *et al.* suggested that deformation can reduce the degree of ordering in these phases giving a decrease in the flow stress with this effect being most significant at the transition temperature for the ordered phase formation, which for Fe-6 wt pct Si steel is around 550 °C.[11,12] No further investigation has been carried out on this matter as it was out of the scope of this paper.

Humphreys *et al.* summarized that mechanical energy is converted into heat, elastic stored energy, and plastic stored energy during plastic deformation.[1] Elastic stored energy is attributed to the residual stress after unloading. Plastic stored energy refers to the crystal defects after deformation, which acts as the driving force of recrystallization. The ratio of the plastic stored energy to the mechanical energy is in the range of 1 to 15 pct for various materials, as reviewed by Titchener and Bever.[13] In this paper, 5 pct was chosen to simplify the calculation, as the purpose is only to compare the stored energy of the uniaxially compressed samples with different deformation temperatures and strains. The absolute values of the stored energy shall be taken with caution. Aravas *et al.* reported that the equation used to estimate the plastic stored energy, E, is given as[14],

$$E = f \int_V \int_0^{\varepsilon} \sigma \mathrm{d}\varepsilon \mathrm{d}V,$$

where f is the ratio of plastic stored energy to mechanical energy, V is the volume of the sample, σ is the true stress level, and ε is the true strain. The calculated stored

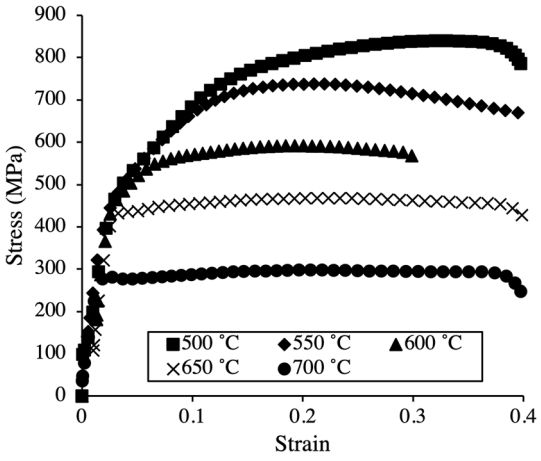

Fig. 2—Flow stress curves of Fe-6 wt pct Si deformed at 500 °C to 700 °C.

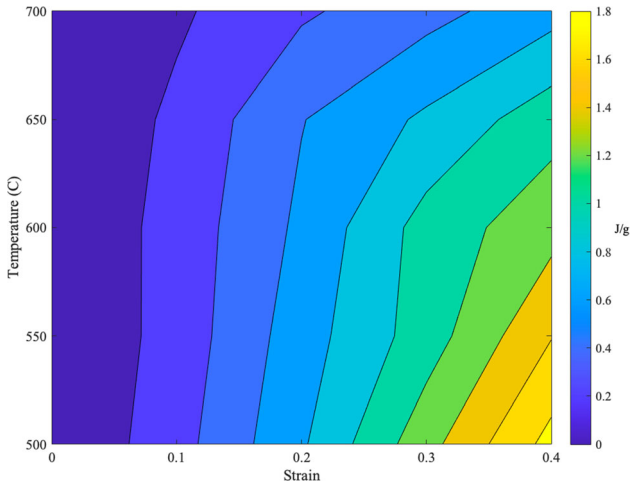

Fig. 3—Stored energy-level estimation based on the flow stress curves.

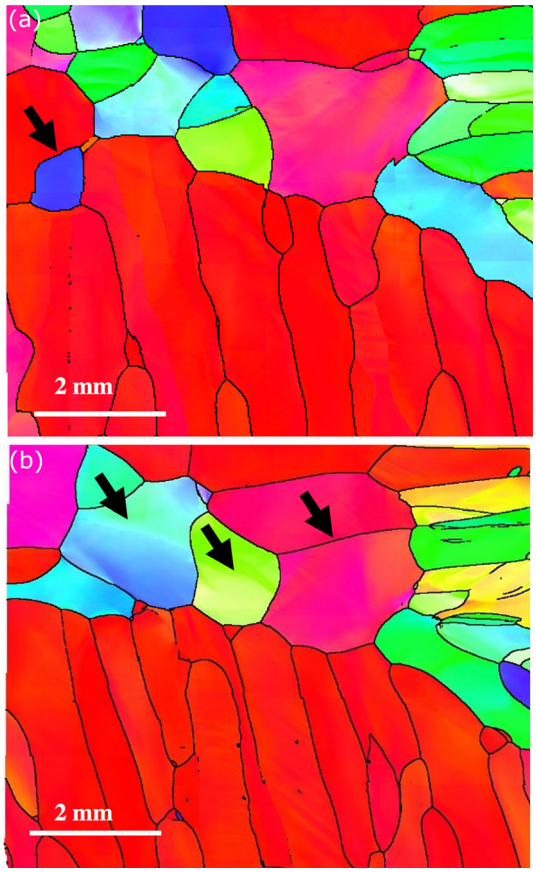

Fig. 4—EBSD IPF *Z* map for the sample deformed at 500 °C, 0.1 strain, strain rate of 1 s^{-1}: (*a*) after deformation and (*b*) the same area after annealing at 1000 °C, 15 min showing recovered, non-recrystallized microstructure.

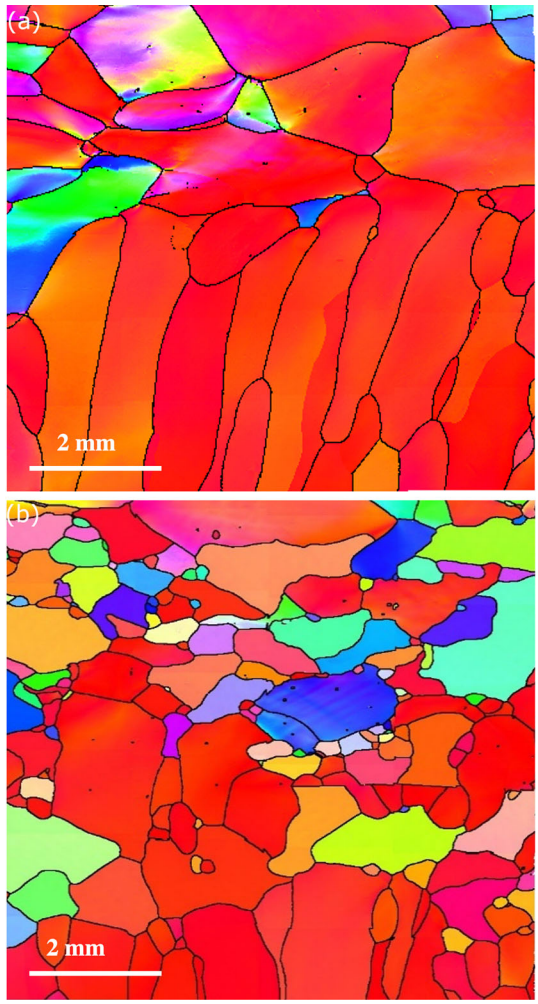

Fig. 5—EBSD IPF *Z* map for the sample deformed at 650 °C, 0.2 strain, strain rate of 1 s^{-1}: (*a*) after deformation and (*b*) the same area after annealing at 1000 °C, 15 min showing recrystallization (69 pct recrystallized) and significant retained {100} texture.

energy mapping is shown in Figure 3. It can be seen that stored energy decreases significantly when the deformation temperature increases above 650 °C. Deformation at 0.1 strain within the temperature range of 500 °C to 700 °C is approximately one magnitude less than at 0.4 strain. Therefore, different softening mechanisms might be expected under these conditions.

Selected examples of EBSD maps after deformation at the various temperatures and strains and after annealing have are shown in Figures 4, 5, and 6. The area fraction of {100}//ND for all three samples after deformation and prior to annealing were determined to be 57 to 60 pct; more details are summarized in Table I. Therefore, the texture change in the three samples after deformation and annealing, especially the {100}//ND area fraction, can only be attributed to recrystallization. Recovery is known to have negligible effect on texture.[15] Examples of SIBM recrystallization nucleation and growth has been shown in a previous paper.[16]

The sample deformed at 500 °C, 0.1 strain is shown in Figure 4. The arrowed regions in Figure 4(b) showed a few localized changes in microstructure, *i.e.*, grain growth, which is attributed to the high annealing temperature process, 1000 °C, 15 minutes. Nevertheless, the area fraction of {100}//ND was kept constant at 60 pct before and after annealing. Also, no formation of new fine and equiaxed recrystallized grains were observed in this case. Therefore, all grains with {100}//ND were retained due to there being insufficient stored energy to promote recrystallization meaning only recovery and grain growth occurred in this case. Figure 5 shows the deformed and recrystallized sample deformed at 650 °C to a strain of 0.2, and then annealed at 1000 °C for 15 minutes. The recrystallized fraction was determined to be 69 pct. It can be seen that there is a high fraction, *i.e.*, 41 pct, of grains with {100}//ND texture, *i.e.*, red colored, which formed during recrystallization. There are very few recrystallized grains with {111}//ND texture (blue color), formed during recrystallization. Figure 6 shows the sample deformed at 500 °C to a strain of 0.4, and then annealed at 1000 °C for 15 minutes. The recrystallized area fraction was 88 pct. It can be seen that the recrystallized grain size is significantly finer than present in the sample deformed at 650 °C, 0.2 strain. This is attributed to the higher stored energy level, which gives a greater number of recrystallization nuclei.[1] Additionally, the recrystallized grains have a more random annealed texture, *i.e.*, significant

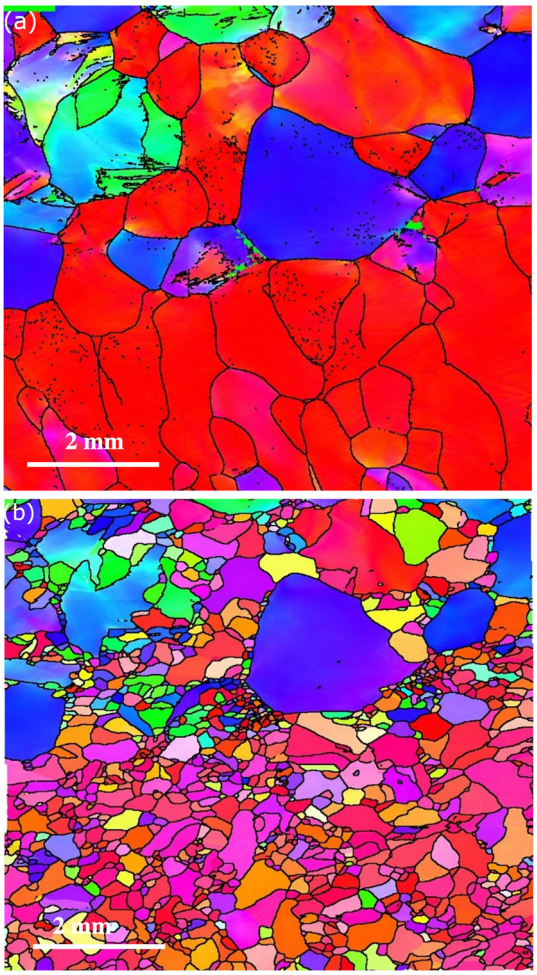

Fig. 6—EBSD IPF *Z* map for the sample deformed at 500 °C, 0.4 strain, strain rate of 1 s^{-1}: (*a*) after deformation and (*b*) the same area after annealing at 1000 °C, 15 min showing recrystallization (88 pct recrystallized) and reduction in {100} texture.

less red colored grains were seen in the recrystallized state. Grains with {100}//ND texture after annealing have decreased to 13 pct.

The area fraction of recrystallized grains with {100}//ND texture under various conditions has been summarized in Table I. Three categories can be observed under these conditions, recovery only, for example, 500 °C and 550 °C at 0.1 strain, due to insufficient stored energy to initiate recrystallization. The area fraction of {100}//ND texture did not change. Secondly, {100}//ND textured grains were favored during recrystallization, *i.e.*, 650 °C at 0.2 and 0.3 strain. Yet the samples were only partially recrystallized after annealing at 1000 °C for 15 minutes due to low stored energy. The third category was the fully recrystallized samples, for example, 500 °C, 0.4 strain, attributed to the sufficient stored energy. These samples also have a random recrystallized texture.

Recrystallization texture is the competition among the recrystallization nuclei with different orientations and their grain boundary mobilities.[17] The texture with a high number density of recrystallization nuclei along with high boundary mobility would be the dominant texture after recrystallization. To promote the less favorable {100}//ND recrystallization texture, a low stored energy state is preferred. The low overall recrystallization nucleation rate leads to the growth of subgrains with less favorable texture, *i.e.*, {100}//ND in this case. As a result, a higher fraction of {100}//ND recrystallization nuclei was formed at low stored energy state. Additionally, an optimum stored energy gradient to promote SIBM recrystallization mechanism could be achieved by controlling the deformation conditions, *i.e.*, 650 °C at 0.2 to 0.3 strain in this case. That is, the stored energy level is sufficiently high to initiate high-angle boundary migration of the recrystallization nuclei and bulging into the neighboring grains attributed to the stored energy gradient. But the stored energy is required to be low enough not to promote the subgrain growth recrystallization mechanism.

In theory, a range of stored energy values after deformation could be identified to promote SIBM recrystallization mechanism, *i.e.*, a combination of deformation temperature and strain level. Firstly, if recovery is sufficiently fast to consume almost all stored energy before the onset of recrystallization, then no recrystallization would occur, nor would the texture change. It is known that the critical strain to initiate static recrystallization increases with increasing deformation temperature. This is attributed to the increasing extent of dynamic recovery during deformation. Secondly, SIBM has been observed to occur in a low stored energy state due to significant differences in stored energy development across grain boundary regions associated with different orientations. With increasing stored energy, the SGG recrystallization mechanism would dominate the recrystallization nucleation process. Then with further increasing in deformation temperature and strain, dynamic recrystallization will be triggered. As a result, a schematic diagram of the effect of strain and temperature on the softening mechanisms can be generated (Figure 7). The shape of the boundaries between recovery, SIBM and SGG recrystallization is determined by the stored energy level, shown in Figure 2. It is worth noting that the boundaries would not be absolute depending on the grain size distribution and texture distribution. Both SIBM and SGG recrystallization would occur under the same deformation condition; these boundaries represent regions where one mechanism dominates.

In addition to the softening mechanisms, the potential for cracking, particularly for the high Si content electrical steels, such as the Fe-6 wt pct Si steel investigated in this work, needs to be considered, which is why warm rolling is favored for these steels. The cracking susceptibility can also be included on the processing map. Processing efficiency considerations can be included, for example, as a minimum strain per pass to achieve final dimensions in an economical manner. These factors are also shown in the schematic diagram in Figure 7.

The processing map concept has been developed for the columnar grain Fe-6 wt pct Si electrical steel and is shown in Figure 8. It can be seen that the processing window for achieving predominantly SIBM recrystallization is small (650 °C at 0.2 or 0.3 strain) but could be

Table I. Area Fraction of {100}//ND Texture Prior and After Annealing at Various Conditions

	Deformed {100}//ND (Pct)	Annealed {100}//ND (Pct)	Recrystallization Fraction (Pct)	{100}//ND in Recrystallized Grains (Pct)
500 °C, 0.1 Strain	60	60	0	0
500 °C, 0.4 strain	57	13	88	13
550 °C, 0.1 Strain	61	61	0	0
550 °C, 0.2 Strain	60	17	69	13
600 °C, 0.2 Strain	58	18	80	17
600 °C, 0.3 Strain	63	15	87	12
650 °C, 0.2 Strain	58	45	69	41
650 °C, 0.3 Strain	52	41	70	29
650 °C, 0.4 Strain	61	36	65	17
700 °C, 0.3 Strain	64	61	3	0
700 °C, 0.5 Strain	53	53	0	0

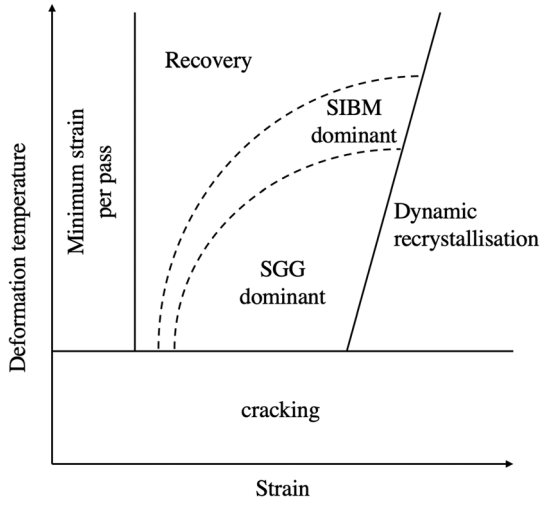

Fig. 7—Schematic diagram of the effect of deformation temperature and strain on softening mechanisms for Fe-6 wt pct Si steel.

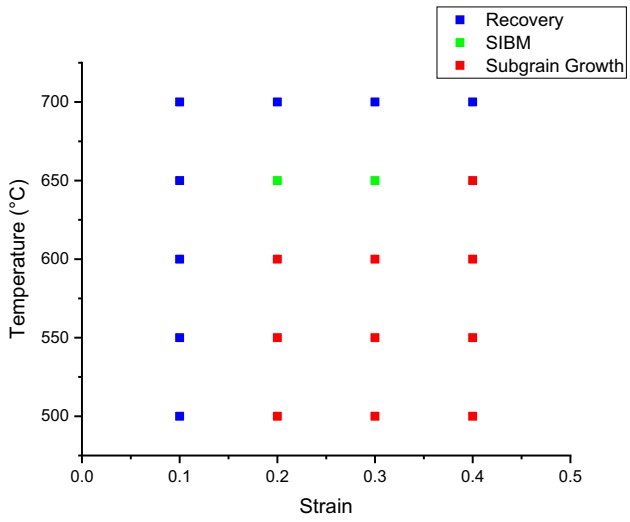

Fig. 8—Processing map for Fe-6 wt pct Si with a strain rate of 1 s^{-1}, initial columnar grain width of 1.2 mm with strong {100}//ND texture, the heating rate at 20 °C/s, annealed at 1000 °C for 15 min.

used to achieve a higher fraction of retained {100} texture during processing if an initial {100} columnar grain structure material (such as formed during twin-roll or belt casting[5]) were to be warm rolled. The SIBM processing window for equiaxed grain structures, such as seen after the initial recrystallization step, needs to be determined for consideration of multi-pass deformation required to achieve the final product. Besides, alternate chemistries (*e.g.*, Si content) could be considered which would change the recovery rates and cracking susceptibility and may allow lower temperature deformation that still achieves the required low stored energy needed to promote SIBM recrystallization. The deformation conditions required to initiate SIBM-dominated recrystallization is within the range of 0.2 to 0.3 strain at 650 °C. No SIBM recrystallization was observed in 550 °C and 600 °C at 0.2 strain, and even comparable stored energy level to 650 °C at 0.2 strain was shown in this case. This could be attributed to the differences in reheating temperatures causing variation in the extent of recovery for these conditions prior to recrystallization, and further investigation is required.

It is worth noting that a fine initial grain size may be required to achieve the desirable final grain size for optimum magnetic performance, *i.e.*, approximately 150 μm, if SIBM recrystallization mechanism is applied to achieve high area fraction of {100}//ND texture as the grain size is not significantly refined with low strain deformation. This is an additional factor that would need to be considered when designing an overall processing route for these steels.

IV. CONCLUSIONS

Uniaxial compression testing of columnar grain Fe-6 wt pct Si electrical steel between 500 °C and 700 °C with strains of 0.1 to 0.4 at a strain rate of 1 s^{-1} has been carried out to determine the recrystallization behavior (strain-induced boundary migration, SIBM, or subgrain growth, SGG) and ability to retain the initial strong {100}//ND texture. It has been found that:

- {100}//ND texture was promoted *via* the SIBM recrystallization mechanism at optimum

deformation conditions, 650 °C, 0.2 to 0.3 strains. A low overall stored energy has been shown to increase the area fraction of the {100}//ND textured grains by SIBM recrystallization mechanism.
- The low area fraction of {100}//ND in the high stored energy samples, such as 500 °C, 0.4 strain, suggested that recrystallization did not retain or favor {100}//ND texture in this case, *i.e.*, random recrystallization texture is produced, which is consistent with SGG recrystallization.
- A processing map concept has been proposed to guide the thermomechanical processing of electrical steels in terms of deformation temperature, strain, and strain rate.

ACKNOWLEDGMENTS

The authors would like to thank EPSRC for funding (Grant Number EP/P01206X/1) and also WMG for their support and facilities.

CONFLICT OF INTEREST

None.

OPEN ACCESS

REFERENCES

1. F. Humphreys and M. Hatherly: *Recrystallization and Related Annealing Phenomena*, 2nd ed., Elsevier, Oxford, 2004, pp. 169–268.
2. J.M. Rosenberg and H.R. Piehler: *Metall. Trans.*, 1971, vol. 2, pp. 257–59.
3. Y. Mo, Z. Zhang, H. Fu, H. Pan, and J. Xie: *Mater. Sci. Eng. A*, 2014, vol. 594, pp. 111–17.
4. F. Humphreys: *Mater. Sci. Forum*, 2004, vols. 467–470, pp. 107–16.
5. M. Takashima, M. Komatsubara, and N. Morito: *ISIJ Int.*, 1997, vol. 37, pp. 1263–68.
6. D. Stojakovic, R. Doherty, S. Kalidindi, and F. Landgraf: *Metall. Mater. Trans. A*, 2008, vol. 39A, pp. 1738–46.
7. F. Fang, Y. Xu, Y. Zhang, Y. Wang, X. Lu, R.D.K. Misra, G. Wang *et al.*: *J. Magn. Magn. Mater.*, 2015, vol. 381, pp. 433–39.
8. H.T. Jiao, W.Z. Xiong, Y.X. Zhang, F. Fang, G.M. Cao, C.G. Li, Y.M. Yu, and Y.B. Xu: *Procedia Eng.*, 2017, vol. 207, pp. 2078–82.
9. Y. He, M. Mehdi, E.J. Hilinski, and A. Edrisy: *IOP Conf. Ser. Mater. Sci. Eng.*, 2018, vol. 375, p. 012013.
10. R. Song, D. Ponge, D. Raabe, J.G. Speer, and D.K. Matlock: *Mater. Sci. Eng. A*, 2006, vol. 441, pp. 1–17.
11. H. Liu, Y.F. Liang, W. Yang, F. Ye, J.P. Lin, and J.X. Xie: *Mater. Sci. Eng. A*, 2015, vol. 628, pp. 262–68.
12. S. Wen, C. Han, B. Zhang, Y. Liang, F. Ye, and J. Lin: *Metals*, 2018, vol. 8, p. 186.
13. A.L. Titchener and M.B. Bever: *Prog. Met. Phys.*, 1958, vol. 7, pp. 247–338.
14. N. Aravas, K. Kim, and F.A. Leckie: *J. Eng. Mater. Technol.*, 1990, vol. 112, pp. 465–70.
15. K. Huang, K. Marthinsen, Q. Zhao, and R.E. Loge: *Prog. Mater. Sci.*, 2018, vol. 92, pp. 284–359.
16. M. Ji, C. Davis, and C. Slater: *J. Phys. IOP Conf. Ser.*, 2019, vol. 1270, p. 012009.
17. W.B. Hutchinson: *Acta Metall.*, 1989, vol. 37, pp. 1047–56.